Dynamic Characterization of Composite Liner-less Tank with Geodesic-Isostrain Dome Contour

Open Access

Akshay Ranjan Pathak[1,*], S.B. Kandagal[2]

1   Department of Aerospace Engineering, Indian Institute of Science, Bengaluru, India
2   Vibrations & Acoustics Lab., Department of Aerospace Engineering, Indian Institute of Science, Bengaluru, India

ARTICLE INFO	ABSTRACT
	The article describes the design, realization and experimental methodology to determine the modal parameters for the composite liner-less tank, which plays an important role in the study of the structural response of the tank. The design of composite liner-less tank is determined by the strain's transverse to the direction of the fibres, and the tank must be able to contain the pressurized fluid without leakage under all given loading conditions. In the present work, a geodesic-Isostrain dome contour for a liner-less carbon epoxy composite tank is determined. The tank is realized by filament winding using an epoxy resin system on a 4-axis CNC filament winding machine. The calculated value of the modal assurance criteria (MAC) for the 1st natural mode is 0.802275, which validates the finite element modelling and analysis approach for the realized tank. To determine the damping coefficient, free vibration tests were performed at the specimen level. The damping coefficients for the tank and the 90-degree specimens agree well, indicating that the resin system determines the damping of the tank in free –free condition. The tank was successfully pressurized to 12 bars with no leakage. The impulse hammer excitation method was used to determine the natural frequencies at different pressure values and found comparable with the finite element simulation results.

1. Introduction

The propellant tank of a spacecraft occupies the most volume and has the largest weight fraction in a propulsion system [1]. Therefore, an optimized storage tank leads to better endurance and performance of the propulsion system. The use of composite materials plays an important role in optimizing the propellant tank in terms of mass, realization time, and avoidance of material wastage.

_____

Due to their higher specific properties and adaptability to requirements, they save a lot of cost and effort. Filament winding is a processing technique in which the fibers are impregnated with resin and wound around a mandrel. Depending on the requirement, the product is made with helical, hoop layers and cured with or without heat and pressure [2].

The 4-axis filament winding machine used to produce the tank under study using the wet winding process is shown in Figure 1. The critical process parameters for filament winding are the winding tension, the processing temperature for the resin, the resin take-up and the winding speed.
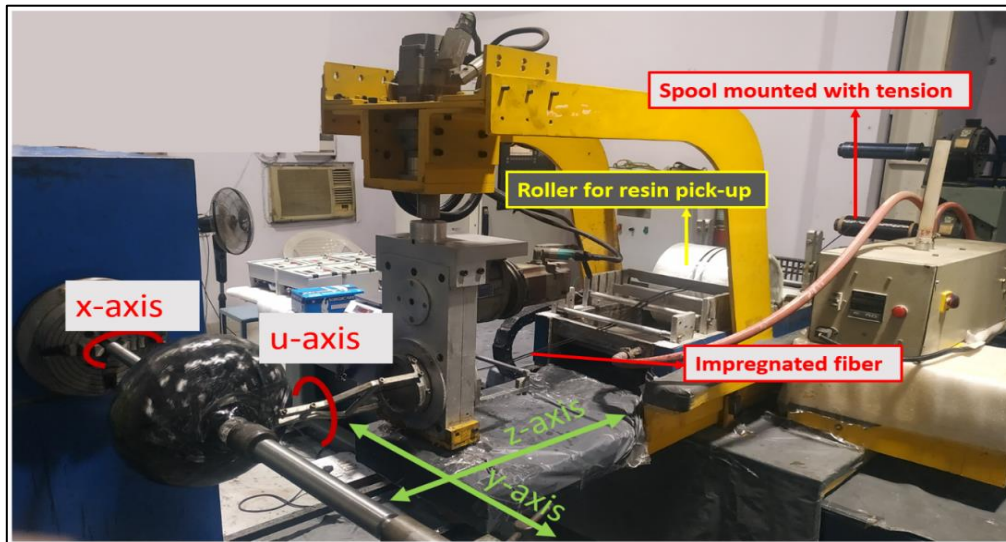

Fig. 1. Filament winding setup for the realized tank

The classification of pressure vessels is shown in Figure 2 [3]. Type I pressure vessels are made of metals and are manufactured using various fabrication processes. Type II pressure vessels are made of metals and have composite jacketing only in the cylindrical area to reduce weight by ring reinforcement in the cylindrical area. Type III pressure vessels have a metallic lining with a composite material wrap with hoops and spirals. Type IV pressure vessels have a plastic lining with composite reinforcement in the hoop and spiral directions. Plastic liners are used to reduce the manufacturing cost and weight of the liner or when the stored fluid is not compatible with the composite wrap of the metal liner. Type V pressure vessels are a new generation of composite pressure vessels in which the composite shell acts as a permeation membrane and can also withstand the pressure loads.

The propellant tank must perform three main functions: maintain internal pressure, serve as a permeation barrier to prevent leakage, and carry environmental and launch loads. Most current composite pressure vessels fall under the type III or IV classification [4]. Type III and IV tanks use a composite overwrap of continuous wound fibers with a resin system over a plastic/metal liner. These liners serve as the primary shape over which composite reinforcement is placed and act as a permeation barrier to the composite pressure vessel. For low temperature, low pressure liquid storage, the performance factor, defined as the energy storage per unit mass (pressure*volume/mass) of type- III /type IV, is significantly lower compared to a composite vessel without a liner [5]. The difference in the coefficient of thermal expansion of liner and composite is another problem that can be overcome by realizing a composite liner-less tank. In contrast, Type V pressure vessels represent a new generation of composite pressure vessels in which the composite shell acts both as an impermeable membrane and supports the structural loads.

Fig. 2. Classification of pressure vessels

In this work, a type V composite pressure vessel with carbon epoxy is realized by filament winding on a dissolvable mandrel with a geodesic-Isostrain dome contour generated based on geodesic conditions and shells of revolution. A tank-free vibration is performed to obtain modal parameters. Finally, the vibration characteristics of the tank under pressure conditions are determined and found to be in good agreement with the predicted finite element results.

A Ø2.4 m composite liner-less tank fabricated by Boeing using automatic tape placement and an autoclave process serves as motivation for the current work. The tank was fabricated from 5320-1 epoxy resin/ with IM -7 carbon fibre composite and successfully tested up to 4 bar internal pressure with 5300με in the transverse to fibre direction strains. The composite tank resulted in a 30% weight reduction compared to the metal tank and reduced the manufacturing cost by 25% [6].

An integrated systematic approach by Mallick et.al [7] describes an interdisciplinary and multi-scale methodology for the development of composite liner-less tanks. The study outlines the methodology for material synthesis, composite laminate modelling, material testing, and tank fabrication and testing. There are very few resources on composite liner-less tanks with not many experimental details on the dynamic response of liner-less tanks. The experimental data and observations will provide a detailed insight into the dynamic response of liner-less tanks, which will be helpful for the efficient design of type V composite tanks.

2. Design & Realization

2.1 Design

Composite pressure vessels are shells of revolution described by the shell theory, which is based on the general theory of membrane stresses in vessels under internal pressure [8]. In addition to the shell theory, other conditions are required for the efficient design of filament-wound composite pressure vessels to obtain different dome contours. The main feature of filament-wound composite pressure vessels is that the fibers are aligned along the resultant of the stresses acting on the vessel wall [9]. Shells of revolution can be represented by Eq.1 [8].

$$\frac{Nx}{r1} + \frac{N\theta}{r2} = p \tag{1}$$

where,

$Nx/N\theta$: Meridional/Circumferential intensity

$r1/r2$: Meridional/Circumferential radius of curvature

p : Internal pressure

Consider a filament wound shell as shown in Figure 3. The shell dome contour is characterized by the radius (r=r[z]) and dome height (z). The stress resultants in principal directions under internal pressure (p) are given by Eq.2

$$Nx = \frac{p\,r2}{2} \; ; \; N\theta = \frac{p\,r2}{2}\left(2 - \frac{r2}{r1}\right) \; ; \; \frac{N\theta}{Nx} = \left(2 - \frac{r2}{r1}\right) \tag{2}$$

$$r1 = \frac{-(1+r'[z]^2)^{\frac{3}{2}}}{r''[z]} \; ; \; r2 = r * \sqrt{(1 + r'[z]^2)} \tag{3}$$

A geodesic line represents the shortest distance between two points on the surface. The flexible fibre placed under tension on the surface takes the shape of a geodesic line, and this property provides stability to the fibre during winding. These are the main properties of a geodesic line over the desired surface. The equilibrium condition for a shell reinforced with flexible fibers loaded with an internal pressure (p) is given by Clairaut's equation [9], which is given in Eq. 4.

$$r \sin \varphi = r_0 \tag{4}$$

where,

r0 : Minimum winding radius

r : Instantaneous radius

R : Maximum winding radius

As the name implies, the geodesic-Isostrain dome shows the same strains in principal directions. Microcracking in the matrix is a strain-dependent failure phenomenon, and the design is governed by the strain transverse to the fibre direction [7].

For the membrane analysis of a shell loaded with internal pressure, the relationship between principal stresses and principal strains is determined using the classical laminated plate theory (CLPT) according to Eq. 5. In this context, only in-plane loads and stiffnesses are considered [7].

$$\begin{Bmatrix} Nx \\ N\theta \\ Nx\theta \end{Bmatrix} = \begin{pmatrix} A11 & A12 & A13 \\ A21 & A22 & A23 \\ A31 & A32 & A33 \end{pmatrix} \begin{Bmatrix} \varepsilon x \\ \varepsilon \theta \\ \gamma x\theta \end{Bmatrix} \tag{5}$$
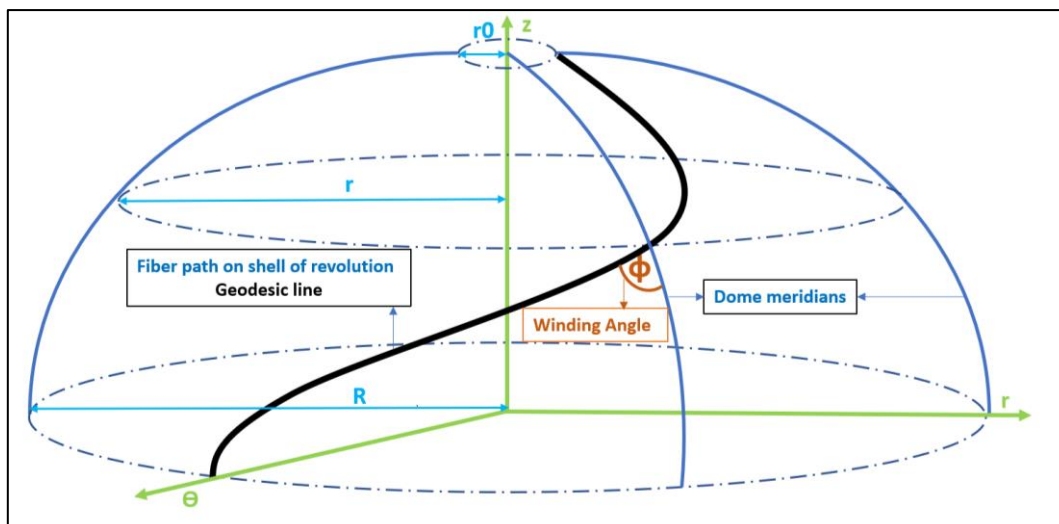
Fig. 3. Geodesic line on a surface of revolution and winding angle

Where A11, A12, A21, and A22 are the in-plane laminate stiffness and εx, εθ are the strains in the principal direction. γxθ is an in-plane shear strain of the laminate. For thin pressure vessels, shear strains are zero (γxθ =0) and for the iso-strain condition (εx= εθ =ε), therefore Eq. 5 is converted to Eq. 6 [5].

$$\begin{Bmatrix} Nx \\ N\theta \end{Bmatrix} = \begin{Bmatrix} A11 & A12 \\ A21 & A22 \end{Bmatrix} \begin{Bmatrix} \varepsilon \\ \varepsilon \end{Bmatrix} \tag{6}$$

Using equations 2 through 6 and substituting the values of r2 and r1, we obtain a second-order differential equation with boundary conditions for the geodesic-Isostrain dome contour given by Eq. 7.

$$r[z]*r''[z] = (2 - (\frac{A12+A22}{A12+A11})) * (1 + r'[z]^2)$$
$$r[0] = R \ \& \ r'$$
$$[0] = 0 \text{ (boundary conditions)} \tag{7}$$

The obtained dome profile for the geodesic-Isostrain condition is shown in Figure 4 (axes are normalized with respect to the maximum radius R). An inflection point is observed at 0.63 (z/R), which can be seen in the tangent and second derivative plots in Figure 5 and Figure 6, respectively. Metallic end fittings are configured from this point or before this point to r0 (minimum radius of filament winding).

The change in slope in the second derivative for the geodesic-Isostrain dome is observed at point 0.5 (z/R), which affects the curvature r1 in the meridian direction and, thus, the intensity of the circumferential load.

The tank was constructed using a carbon epoxy composite for the derived shell, and EN -8 steel end fittings and closures were used. The design inputs are shown in Table 1.
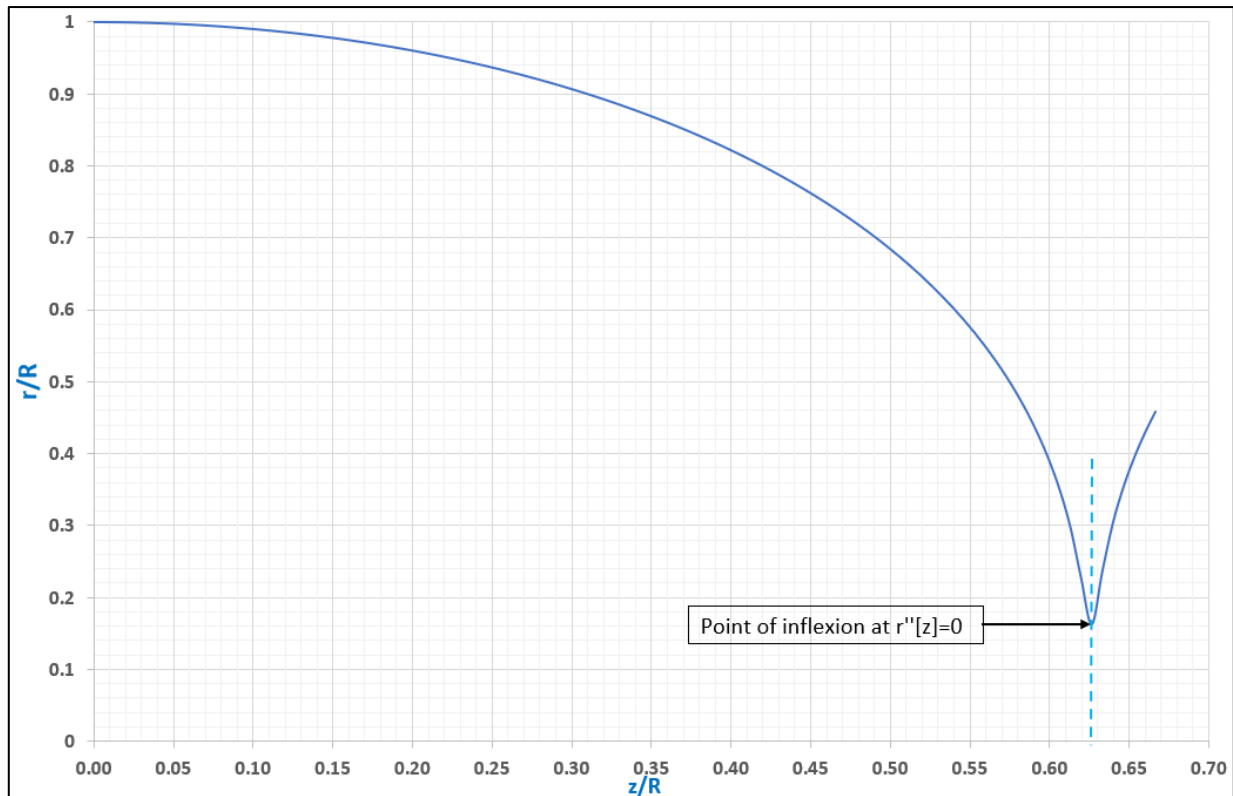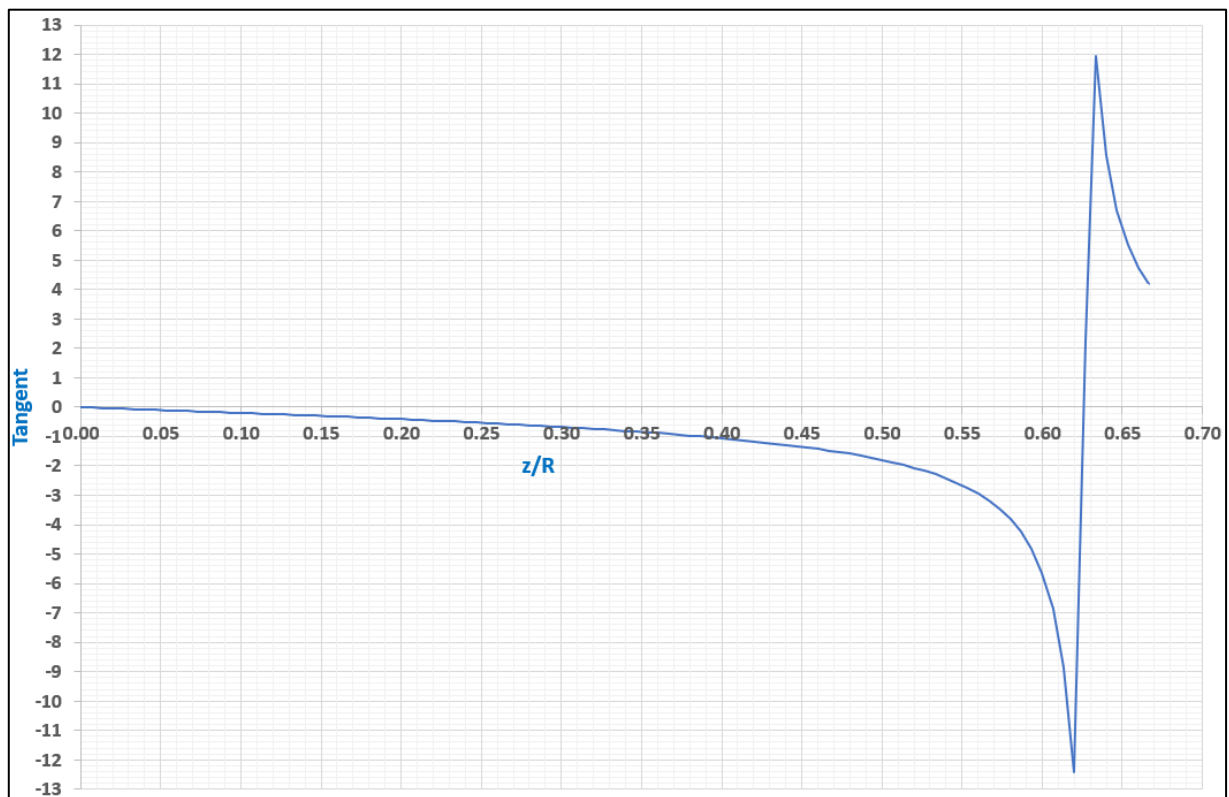
Fig. 4. Geodesic-Isostrain dome meridian profile

Fig. 5. Tangent variation for Geodesic-Isostrain dome
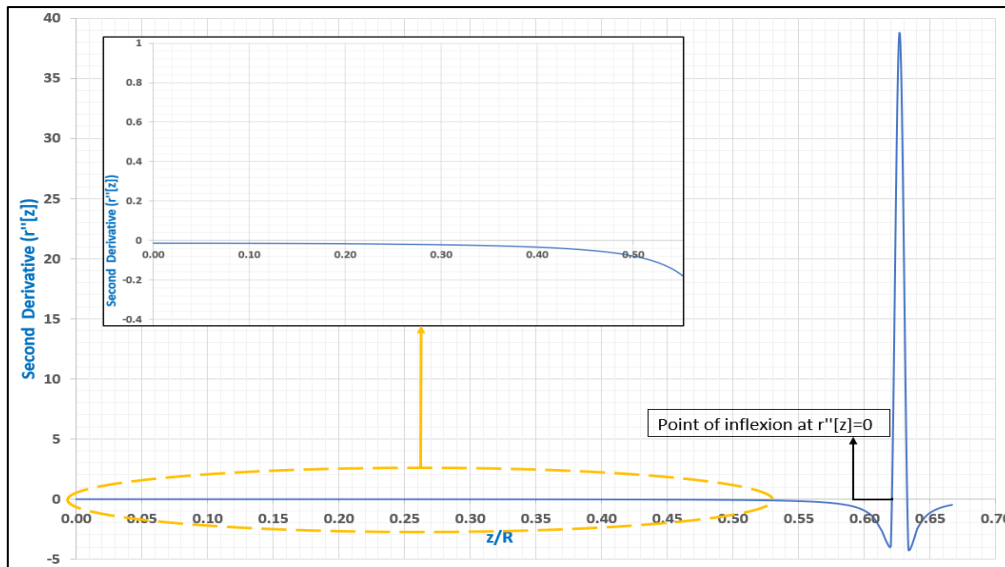
Fig. 6. Second derivative variation for Geodesic-Isostrain dome

2.2 Realization

The tank consists of 3 double helical layers, 2 of which are stepped back layers and was fabricated on a dissolvable thermocole mandrel using a 4-axis CNC filament winding machine. Commercially available filament winding software CADFIL was used to generate the winding program. The curing cycle followed is 24 hours at room temperature followed by 8 hours at 40°C in an oven. After winding and curing, the thermocole mandrel was dissolved with acetone. Each layer fiber path obtained through CADFIL and the stages of tank realization are shown in Figure 7 and Figure 8, respectively.
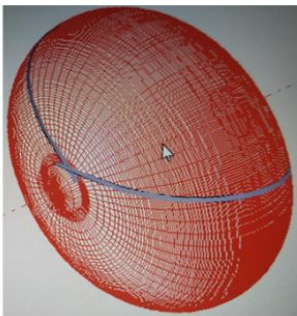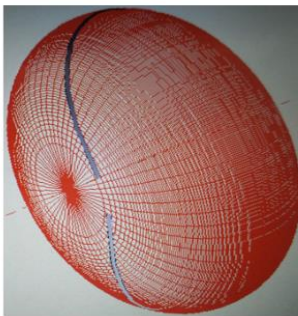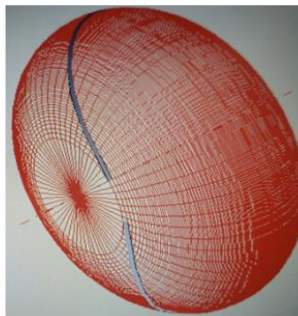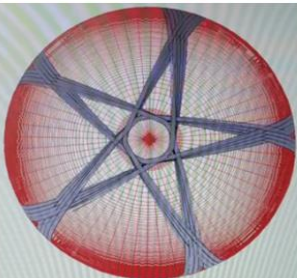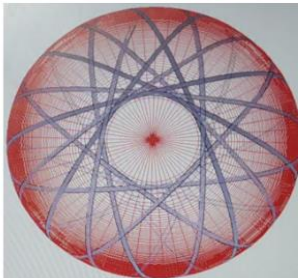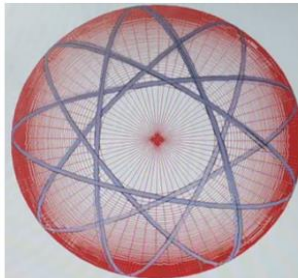

Fig. 7. CADFIL fiber path and winding pattern

Table 1
Material properties and design input

Description	Value
Composite	
E1 (Fiber direction Modulus)	140,000 MPa
E2 (Transverse direction Modulus)	4,000 MPa
μ12 (Poisson's ratio)	0.26
G12, G13 (Shear Modulus)	2,700 MPa
G23 (Shear Modulus)	1,538 MPa
Density	1,600 kg/m^3
Ply thickness	0.35 mm
Transverse micro strain (Failure Limit)	2,000
The factor of safety on transverse strain	2
End Fitting & Closure	
Young's Modulus	200,000 MPa
Density	7,800 kg/m^3
Shell Inputs	
r0 (Min. radius of winding)	25 mm
R (Max. radius of winding)	150 mm
Design Pressure	10 bar
Design Volume	9 Liter
Winding Mandrel	
Material	Thermocole
Density	22 kg/m^3

3. Experimental Setup

Several tests were performed on the specimen level and tank [10] sample to evaluate various parameters required for the finite element simulations. The details of the experimental tests are summarized in Table 2, and the experimental setups for various tests are shown in Figure 9.
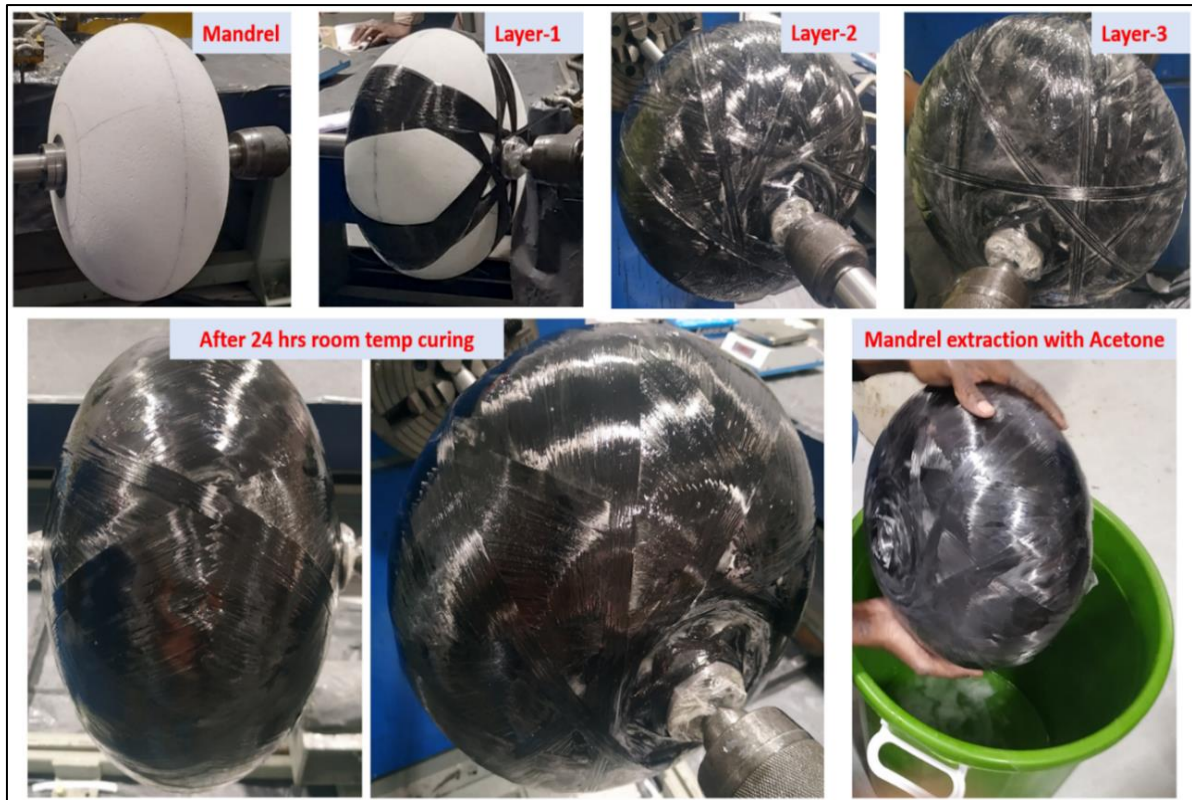
Fig. 8. Tank winding and realization

Table 2
List of experimental tests and their objectives

Type of Test	Test specimen	Objective of the Test
Free vibration (Cantilever beam configuration)	0-degree specimen As per ASTMD-3039	To evaluate fiber direction co-efficient of damping.
Free vibration (Cantilever beam configuration)	90-degree specimen As per ASTMD-3039	To evaluate transverse to fiber direction co-efficient of damping.
Radiography	As wound tank	To assess the thickness buildup and distribution near end fitting.
Free Vibration	As wound tank	To obtain modal parameters & validate the FE simulations.
Vibration test with internal Pressure	As a wound tank with end closures	To ensure leak tightness and to obtain natural frequencies at different pressure levels.

Fig. 9. Experimental test setup

4. Simulation and Experimental Results

i.   Finite element simulation is performed using the commercially available software Abaqus and a shell model is generated for analysis and simulation. For a filament wound composite pressure vessel, the thickness and winding angle change continuously as we move from r=R to r=r0 (i.e., from the cylinder to the pole opening). In addition, the thickness formed near the end-fitting region is highly dependent on the process parameters. Therefore, a continuous change in the winding angle and thickness is simulated. As we move from r=R to r=r0, the winding angle changes, which is determined using Clairaut's law (Eq.4). The variation of the winding angle along the dome is shown in Figure 10.

The thickness changes along the meridian of the dome and is divided into 2 parts. First, from r=R to ra= r0 +2 times the winding bandwidth (based on process parameters). Second, from ra to r0, where the actual thickness built up is recorded using a cubical fit approximation.

 r=R to r=ra

$$t = \frac{(R * t_R * Cos[\varphi_R])}{((r * Cos[\varphi]))}$$

$$\varphi = \text{ArcSin}\left[\frac{r0}{r}\right]$$

(8)

t_R : thickness at r=R t : thickness at a given radius r

φ_R : winding angle at r=R   ɸ: winding angle at given radius r

_r=ra to r=r0_: A cubic fit is used for this region [9], and the variation in thickness is shown in Figure 11. Four conditions are required to estimate the constants of the cubic fit, as explained below.

$\Rightarrow$ Cubic fit equation should satisfy the condition that the thickness at r0 should be equal to t_R.
$\Rightarrow$ Cubic fit equation should satisfy the condition that the thickness at ra should be equal to t as calculated based on eq. 8.
$\Rightarrow$ Tangent continuity at r=ra.
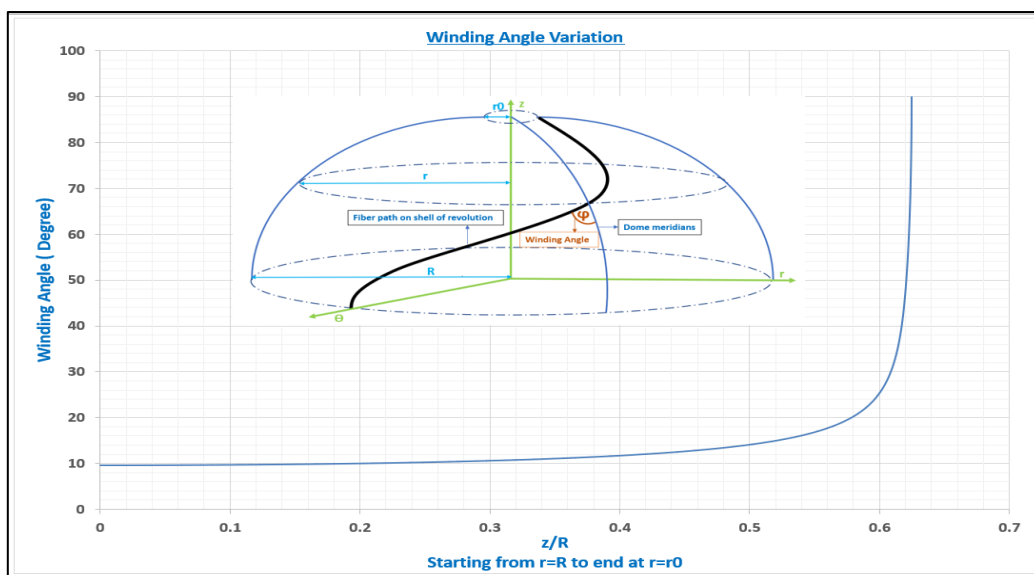$\Rightarrow$ Fiber content remains constant.

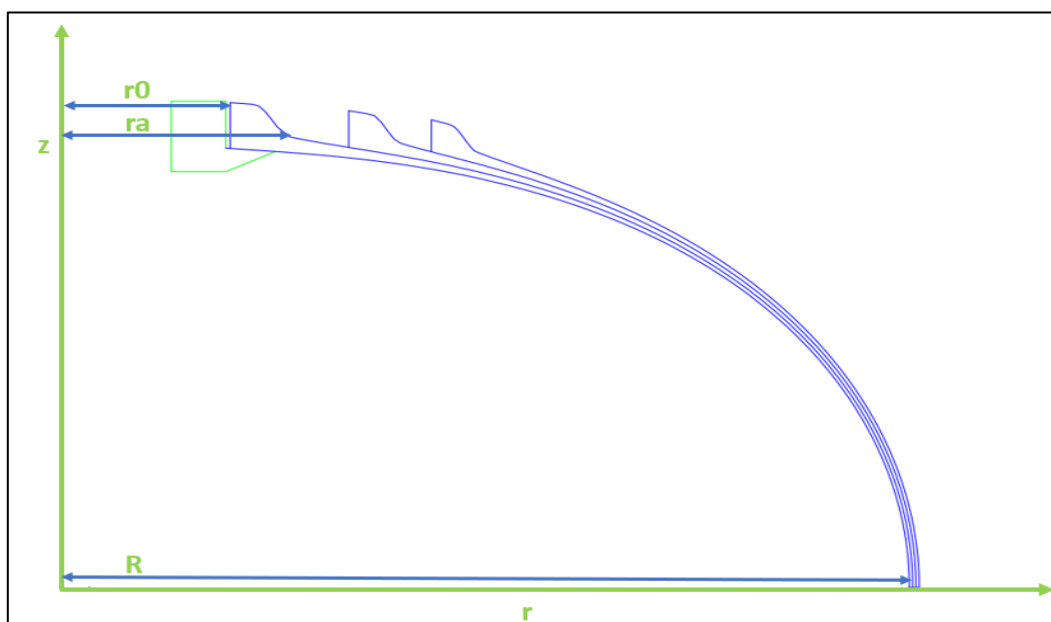**Fig. 10.** Winding angle variation along the dome

Fig. 11. Thickness variation along the dome

ii.   Composite layup has been used for the wound shell, and solid elements are used for the end fitting/closure, as shown in Figure 12. The water mass is modeled as non-structural mass in the simulation. The element type for the composite shell is S4R, general purpose shell elements, and the solid element type for the end fitting, end closure, and water are C3D8R and C3D6. The different shades of color indicate the areas with different cross-sectional properties along the dome.
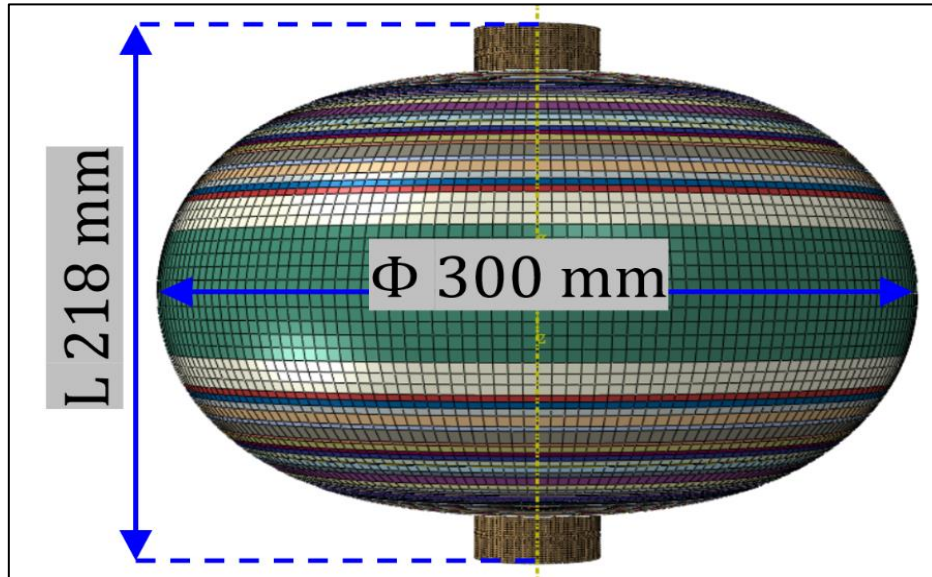

Fig. 12. Tank overall configuration

iii. The acceleration time history for the tensile specimens is shown in Figures 13 and 14. Navaneeth et.al [11] have shown experimentally that the damping coefficient increases with increasing resin content. Since the behavior of the 90-degree specimens is dominated by the resin, a higher damping coefficient is observed.
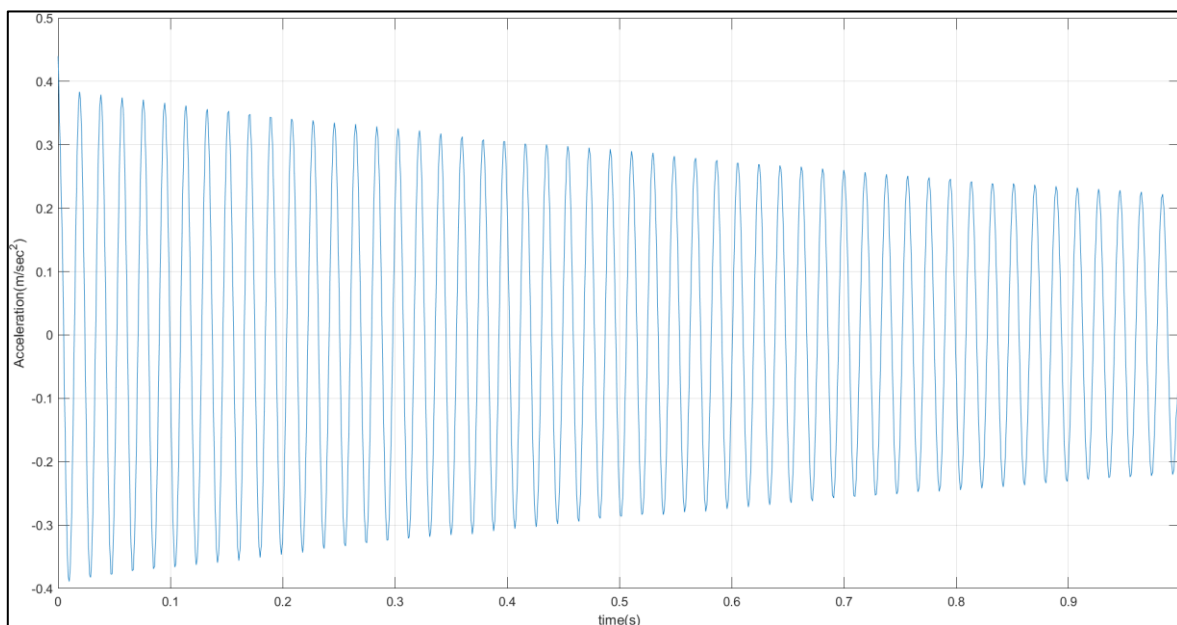

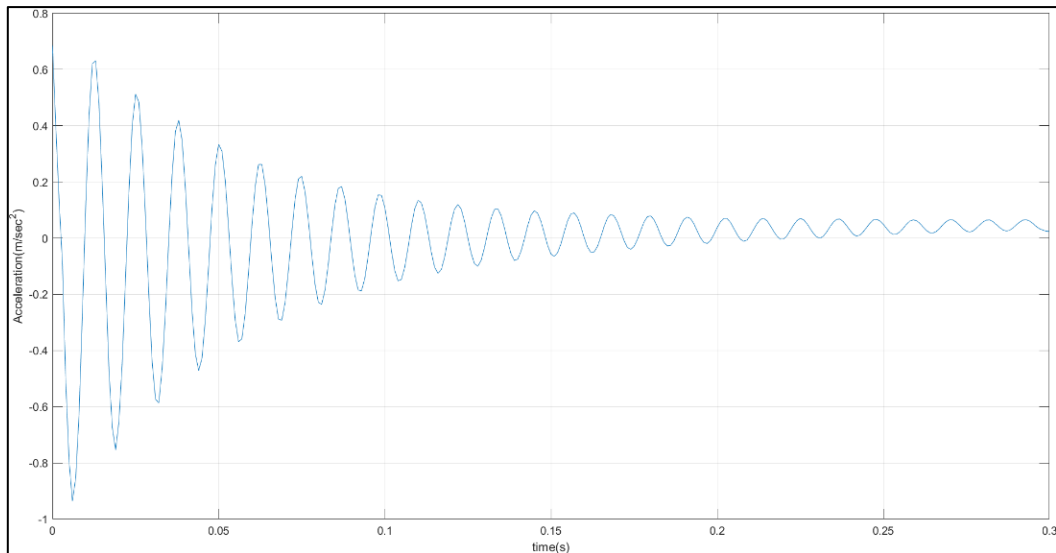**Fig. 13.** The 0-degree specimen time history

Fig. 14. The 90-degree specimen time history

The damping values determined by the logarithmic decrement method are shown in Table 3.

Table 3
Tensile specimen co-efficient of damping

Description	0-degree specimen (Co-efficient of damping)	90-degree specimen (Co-efficient of damping)
Specimen-1	0.0018	0.0346186
Specimen-2	0.0016	0.031472
Specimen-3	0.0016	0.031593

iv.   The simulated thickness is comparable to the realized thickness measured through radiography (Figure 15). Also, the simulated & measured masses are 2 kg and 1.96 kg, respectively validating the simulation approach.
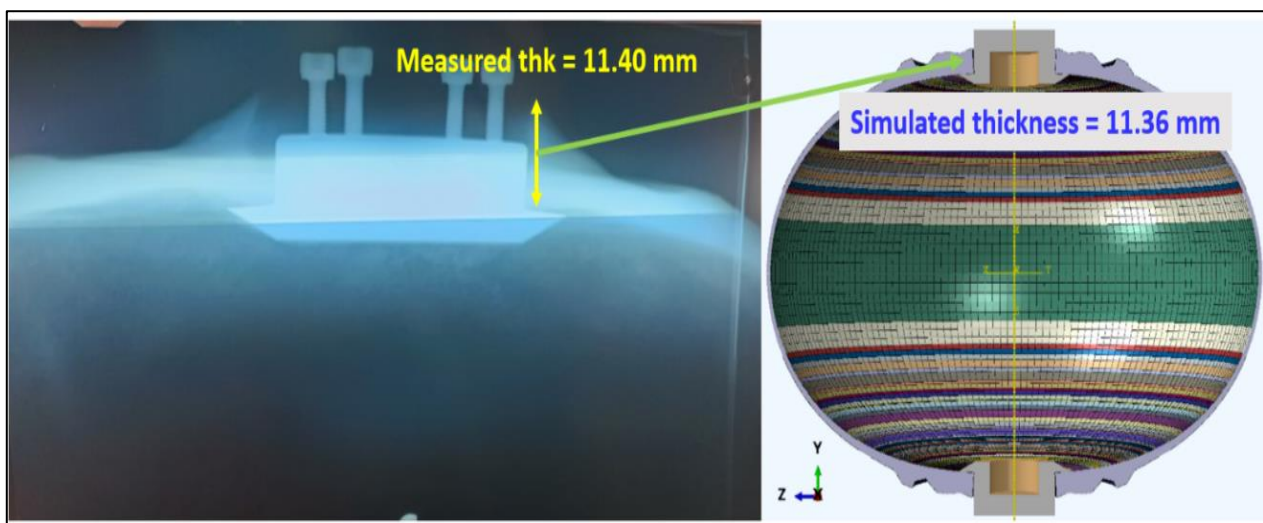

Fig. 15. Simulated and measured thickness (radiography)

v. Realized tank was subjected to free vibration, excitation was provided by impulse hammer, and the accelerometer response was recorded for different locations, as shown in Figure 16.
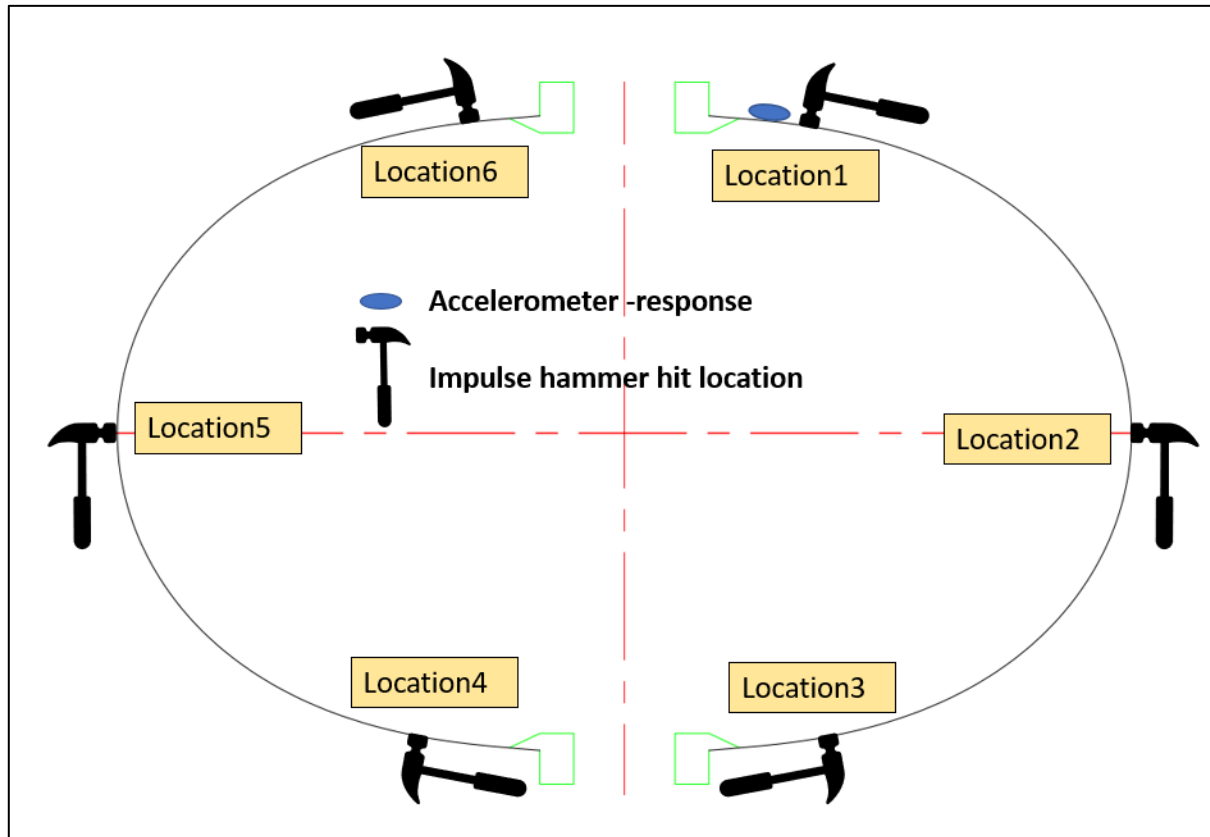

Fig. 16. Response and excitation at different locations on the tank

The damping coefficient (η) is calculated from the real part of the FRF (accelerance) by using the half power bandwidth method [12], using frequencies fa (resonant frequency +3dB) and fb (resonant frequency-3dB) as shown in Figure 17 and the relationship given by Eq.9.

$$\eta = \frac{\left(\frac{fa}{fb}\right)^2 - 1}{\left(\frac{fa}{fb}\right)^2 + 1} \qquad (9)$$

A typical plot obtained from experimental data for the frequency response function (FRF), which is a transfer function expressed in frequency domain and power spectral density (PSD), is shown in Figure 17.

The modal parameters obtained are listed in Table 4 and compared with the finite element simulation (Figure 18).
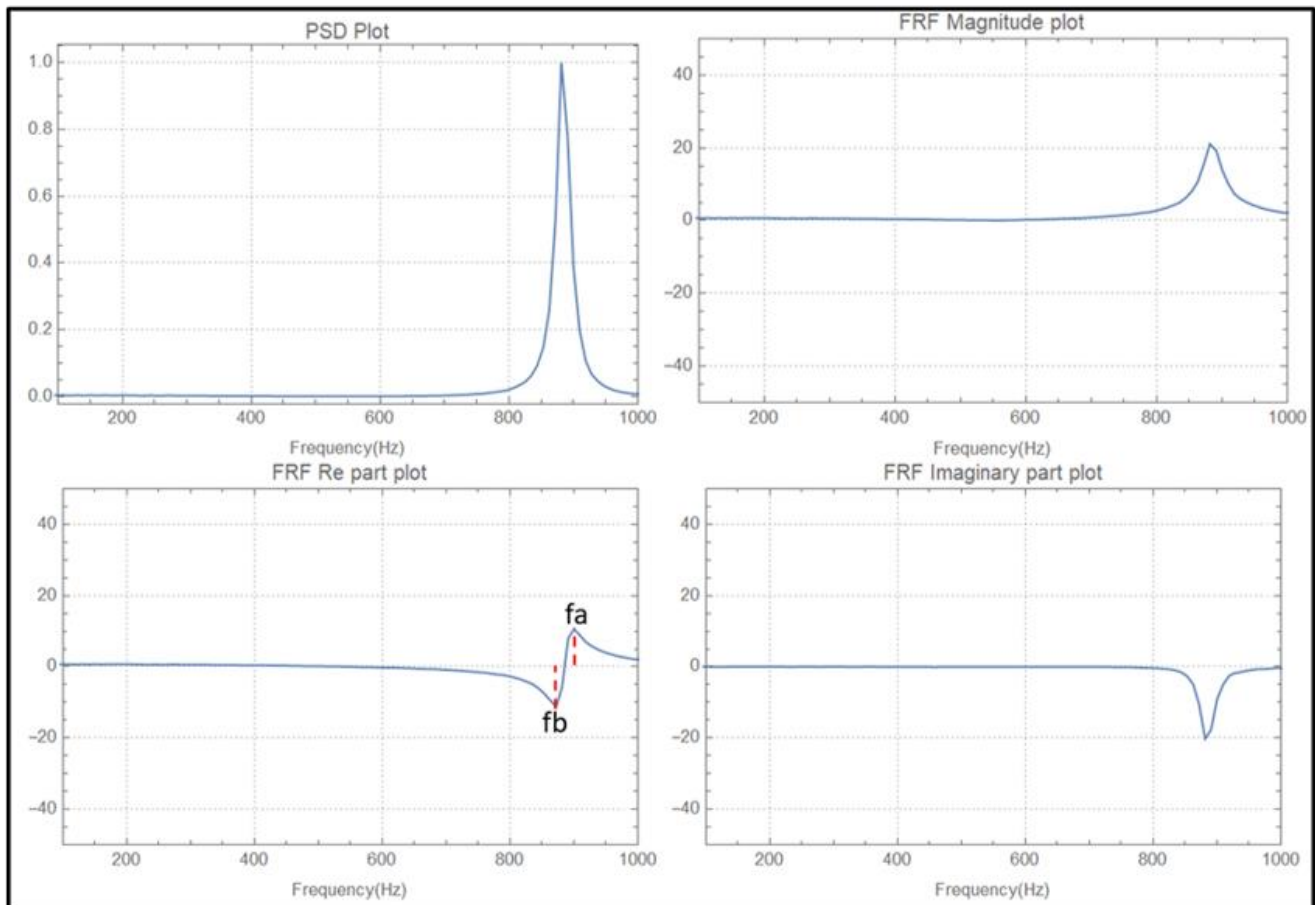
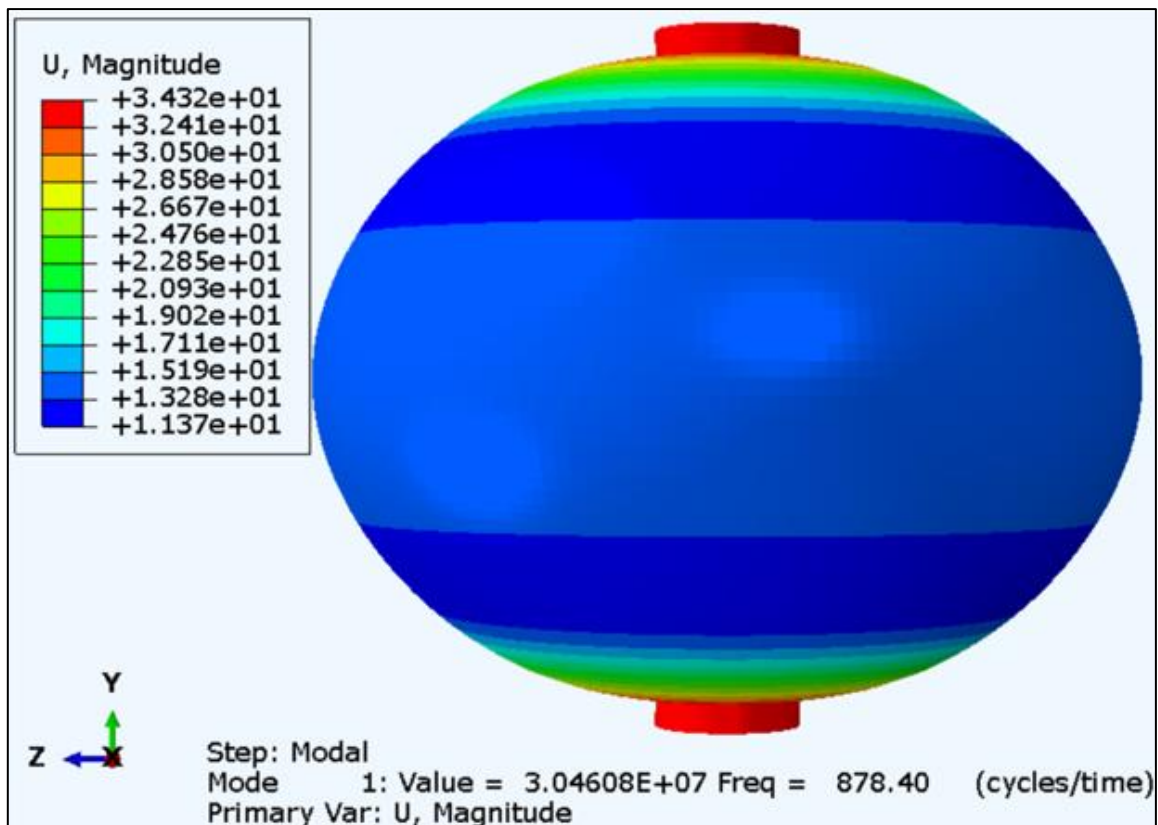**Fig. 17.** Typical PSD and FRF plot obtained from free vibration of tank

Fig. 18. Mode shape and 1st natural frequency for the tank under free-free condition - FE simulation

Table 4
Natural frequencies and co-efficient of damping

Description	Damped Natural frequency (Hz)	Co-efficient of damping	Undamped Natural frequency (Hz)
Location-1	881.85	0.0321643	881.39
Location-2	884.296	0.0290979	883.92
Location-3	883.841	0.0342521	883.32
Location-4	881.538	0.0344204	881.02
Location-5	886.537	0.0318464	886.09
Location-6	884.182	0.0342521	883.66
Average	883.70	0.03235622	883.14

The surface of the tank was divided into 100 grid points to experimentally determine the mode shape. The modal assurance criterion (MAC) is used to calculate the correlation between the experimentally determined mode shape and the simulation at FE. MAC is calculated using Equation 10 [13].

$$MAC = \frac{(Transpose[\psi FE].\psi exp)^2}{(Transpose[\psi FE].\psi FE) * (Transpose[\psi exp].\psi exp)}$$

(10)

ψFE : Modal vector from FE simulation
ψexp: Modal vector from experiment

The calculated MAC value for 1st natural mode is **0.802275**.

vi. The tank was subjected to a hydraulic pressure test up to 12 bar and no leakage was detected in the shell. The layered shell model is used for simulation under pressure and water mass with fixed boundary conditions at one end, as shown in Figure 19. A comparison of the experimentally and simulated natural frequency at different pressure levels is shown in Table 5. As the pressure increases, the natural frequency increases due to the generation of membrane stresses in the shell under pressure loading. Similar behavior is observed in a study on the effect of gas pressure and density on the vibration of a cylindrical pressure vessel by Omid Mir et.al [14] and a study on a composite pressure vessel by Shaojun [15].

5. Conclusions

A liner-less Type V composite tank was designed and realized using a dissolvable thermocole mandrel with a carbon epoxy system and metallic end fittings. A parallel finite element simulation was performed to validate/compare the experimental results. Sample level studies were performed

prior to tank level experiments. Free vibration tests were performed at the specimen level to determine the damping coefficient. The damping coefficient for the tank and 90-degree specimens is similar, indicating that the damping of the tank is determined by the resin. The first natural frequency obtained by simulating FE is 878.40 Hz, which is 0.53% lower than the experimental value of 883.15 Hz (undamped natural frequency). The calculated MAC value for the 1st natural frequency is 0.802275, which confirms the modelling and analysis approach for the realized tank. The natural frequencies obtained during the pressure test at different pressures are close to the values obtained in the FE simulations. An increase in natural frequency with increasing internal pressure is observed in the experiment, and a similar phenomenon is observed in the FE simulation results. As the internal pressure increases, the natural frequency increases due to the generation of membrane stresses in the shell under pressure loading. The tank was successfully pressurized up to 12 bars without any leakage. The study establishes the design methodology and the approach to evaluate the modal parameters for the composite liner-less tank.
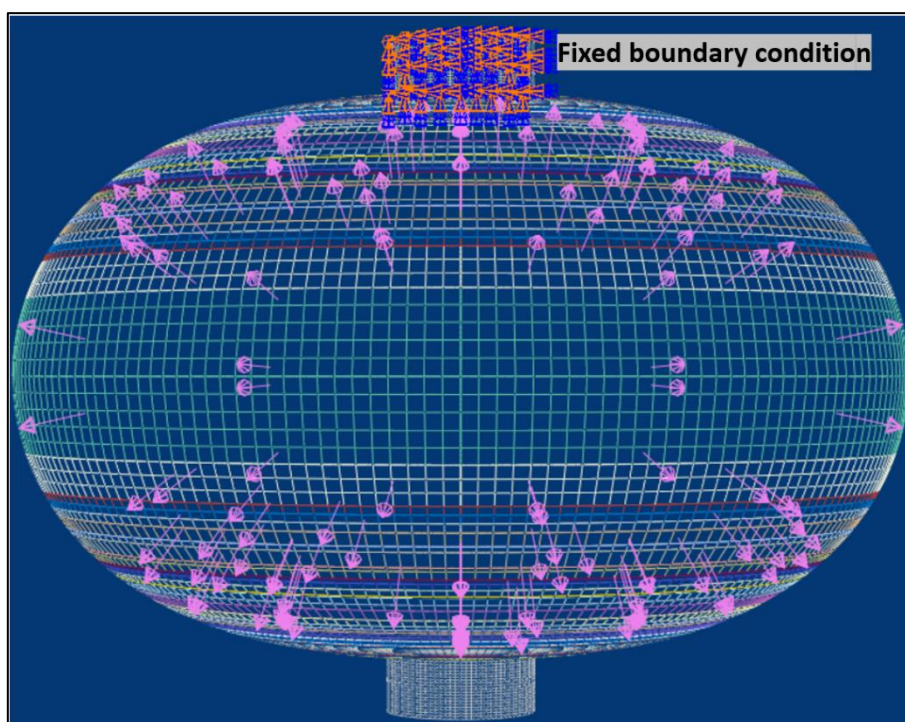

Fig. 19. Shell model - load and boundary condition

Table 5
Natural frequency – FE and experimental

Description	Frequency (Hz) FE simulation	Frequency (Hz) Experiment	Difference (%)
With water mass and no pressure	403.74	400	-0.94
With water mass and 1 bar pressure	405.27	409.09	0.93
With water mass and 2 bar pressure	406.78	411.77	1.21
With water mass and 3 bar pressure	408.28	413.76	1.32
With water mass and 4 bar pressure	409.78	416.66	1.65

References

[1] T. Walter, P. Griffin, A.C. Jackson, "Design and Manufacture of a Composite Overwrapped Pressurant Tank Assembly," 38th AIAA/ASME/SAE/ASEE Joint Propulsion Conference & Exhibit. American Institute of Aeronautics and Astronautics (2023).
https://doi.org/10.2514/6.2002-4349

[2] A.K. Kaw, Mechanics of composite materials, 2nd Edition (Boca Raton: CRC Press, Taylor & Francis, 2006).
https://doi.org/10.1201/9781420058291

[3] Infinite Composites,"Composite pressure vessels resources," (2023).
https://www.infinitecomposites.com/composite-pressure-vessel-resources

[4] Stratview Research, "Hydrogen pressure vessels market forecast 2023 – 2030," (2019).
https://www.stratviewresearch.com/3315/hydrogen-pressure-vessels-market.html

[5] K. Mallick, J. Cronin, S. Arzberger, M. Tupper, L. Grimes-Ledesma, J. Lewis, C. Paul, J. Welsh,"Ultralight linerless composite tanks for in-space applications," Space 2004 Conference and Exhibit, 28 – 30 September 2004, San Diego, California. American Institute of Aeronautics and Astronautics (2004).
https://doi.org/10.2514/6.2004-5801

[6] J.J. Jackson, J. Vickers, J. Fikes, "Composite Cryotank Technologies and Development 2.4 And 5.5m Out Of Autoclave Tank Test Results," NTRS – Nasa Technical Reports Server. Composites and Advanced Materials Expo (CAMX), Dallas TX – Conference Paper ID: 20150021410 (2015).
https://ntrs.nasa.gov/citations/20150021410

[7] K. Mallick, J. Cronin, K. Ryan, S. Arzberger, N. Munshi, C. Paul, J. Welsh, "An Integrated Systematic Approach to Linerless Composite Tank Development," 46th AIAA/ASME/ASCE/AHS/ASC Structures, Structural Dynamics and Materials Conference, 18 – 25 April 2005, Austin, Texas (2005).
https://doi.org/10.2514/6.2005-2089

[8] J.F. Harvey, "Theory and Design of Modern Pressure Vessels," Second Edition, Van Nostrand Reinhold (1974).

[9] V.V. Vasiliev (Edited by R.M. Jones), Composite Pressure Vessels: Design, Analysis, and Manufacturing (Virginia USA: Bull Ridge Publishing, 2009).
https://www.gbv.de/dms/tib-ub-hannover/657179817.pdf

[10] A.R. Pathak, "Structural Response of Liner-Less Composite Tank with Different Dome Contours" (Master Thesis, Indian Institute of Science, Bengaluru, 2022).

[11] M. Navaneeth, S. Poojary, A. Chandrashekar, A. Razak, N. Hasan, A.I. Almohana, "Damped Free Vibration Analysis of Woven Glass Fiber-Reinforced Epoxy Composite Laminates," Advances in Materials Science and Engineering, (2022): 1 – 13.
https://doi.org/10.1155/2022/6980996

[12] T. Irvine, "An Introduction to Frequency Response Functions," Fundamental Notes, (2000): 1 – 14.
http://www.vibrationdata.com/tutorials2/frf.pdf

[13] D.J. Ewins, "Model Validation: Correlation for Updating," Sadhana 25, (2000): 221 – 234.
https://doi.org/10.1007/BF02703541

[14] M. Omid, M. Shakouri, M.R. Ashory, "Gas Pressure and Density Effects on Vibration of Cylindrical Pressure Vessels: Analystical, Numerical and Experimental Analysis," SN Applied Science 2, no. 134 (2019): 1 – 9.
https://doi.org/10.1007/s42452-019-1916-z

[15] Q. Shaojun, "Dynamic Analysis of Composite Overwrap Pressure Vessel" (Master Thesis, Vanderbilt University Institutional Repository, 2004).
https://ir.vanderbilt.edu/bitstream/handle/1803/14740/thesis-shaojun.pdf?sequence=1&isAllowed=y